ACS APPLIED MATERIALS & INTERFACES

Research Article

www.acsami.org

Plasmon-Induced Photoluminescence Immunoassay for Tuberculosis Monitoring Using Gold-Nanoparticle-Decorated Graphene

Jaewook Lee,[†,‡] Jeonghyo Kim,[†] Syed Rahin Ahmed,[†] Hongjian Zhou,[†] Jong-Man Kim,[†] and Jaebeom Lee*[,†]

[†]Department of Nano Fusion and Cogno-Mechatronics Engineering, Pusan National University, Busan 609-735, Republic of Korea

[‡]Department of Mechanical and Manufacturing Engineering, University of Calgary, Calgary T2N 1N4, Canada

Supporting Information

ABSTRACT: Metal-nanoparticle-functionalized graphene, in particular, graphene sheets containing Au nanoparticles (Au NPs), have generated considerable interest because of their unique optical and electrical characteristics. In this study, we successfully produced graphene sheets decorated with Au NPs (AuGrp) using phytochemicals as reducing agents. During this reaction, Au ions intercalated into the layered graphene flakes and were then reduced into NPs, exfoliating the graphene sheets. The physicochemical properties of the AuGrp nanocomposites were characterized, and the exfoliation process was investigated using a molecular dynamics simulation of Au NPs between graphene sheets. Our proposed technique is advantageous because the phytochemicals are mild reducing agents that preserve the graphene structure during exfoliation and NP decoration. The dispersity of the NPs on the graphene sheets was drastically improved due to the use of metal-ion intercalation. Moreover, the electrical conductivity was 6−30 times higher than that of bare graphene and reduced graphene oxide. Using antibody (Ab) modified AuGrp sheets and quantum dots, a plasmonic-induced photoluminescence immunoassay of tuberculosis (TB) antigen (aG) CFP-10 was demonstrated for a potential application of these materials. The enhancement of photoluminescence (PL) response was monitored depending on the various TB aG concentrations from 5.1 pg/mL to 51 μg/mL, and the detection limit for CFP-10 was 4.5 pg/mL. Furthermore, the selectivity was demonstrated with Ag85 as the other TB aG, and PL enhancement was not observed in this case. Therefore, AuGrp-based immunoassay showed the potential for biosensor application.

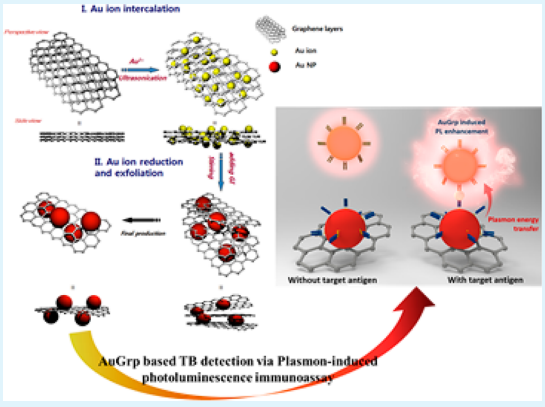

KEYWORDS: *Au-decorated graphene, mild reduction conditions, plasmon resonance energy transfer, tuberculosis sensing, plasmon-induced photoluminescence*

INTRODUCTION

Since the original development of graphene, variants such as functionalized graphene have attracted considerable attention as candidate materials for applications in optoelectronics,[1,2] biosensors,[3,4] and nanoelectronics.[5] Among the different types of functionalized graphene, graphene sheets decorated with gold nanoparticles (NPs), or AuGrp, have received special interest by virtue of their electrical properties, Raman scattering signal, catalytic behavior, surface plasmon resonance (SPR) characteristics, and potential biological applications.[4,6,7] Graphene possesses π electrons and oxy-functional groups, i.e., carboxylic, hydroxyl, and epoxy groups, and thus Au ions can be easily adsorbed onto the graphene surface.[8−10] Therefore, AuGrp can be fabricated using solution-based processes.

Several methods have been introduced to fabricate AuGrp. One well-known method involves the use of harsh chemicals, e.g., sodium borohydride to reduce $HAuCl_4$ and/or thiolic chemicals for NP stabilization, to deposit Au NPs onto graphene surfaces.[4,11] Microwave-assisted methods are an alternative to these chemical treatments, however the reaction requires one or 2 days.[10,12] Thermal processes can also be used to assist Au-NP deposition onto graphene; these methods typically require a temperature of about 100 °C and a few hours of stirring.[13,14] The decoration of graphene with Au NPs by electrochemical deposition is more complicated than by other methods.[7,15]

Recently, nanocomposites incorporating different types of nanomaterials have been studied extensively because of the richness and tunability of their optical and electronic properties compared to those of their individual components, and fabricating nanocomposites incorporating graphene sheets in order to improve the electrical characteristics of the sheets is a goal of recent research. Phytochemicals have been utilized as reducing agents in many nanocomposite applications.[16]

Received: September 17, 2014
Accepted: November 14, 2014
Published: November 14, 2014

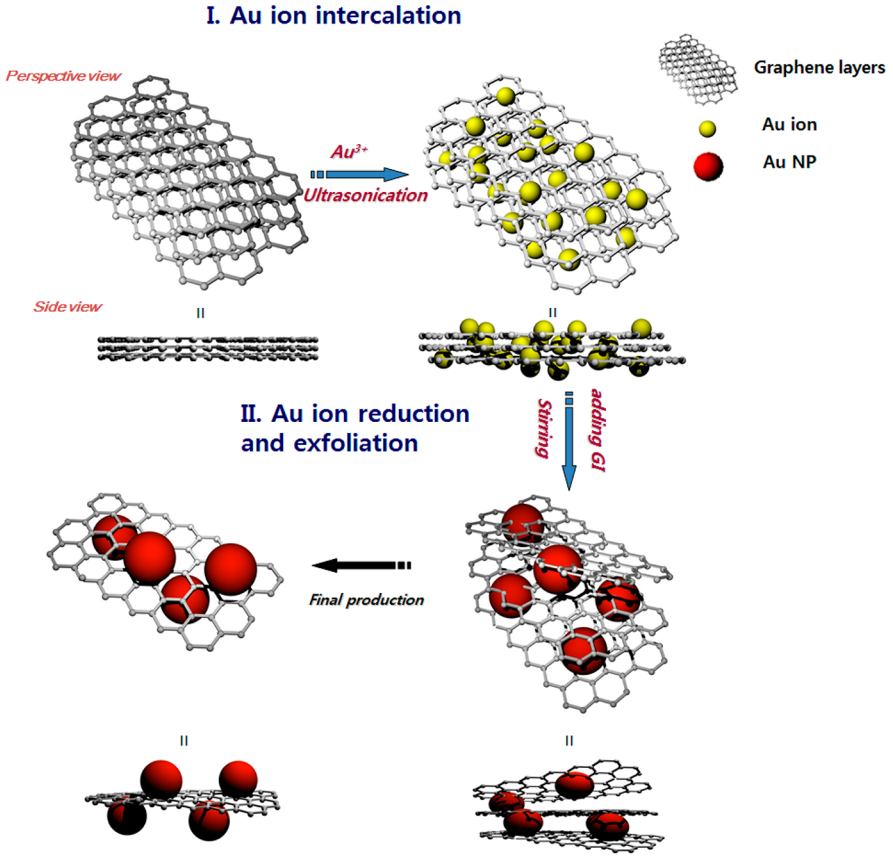

Figure 1. AuGrp fabrication process. A schematic illustration of (I) the intercalation of Au ions into the graphene flakes, and (II) the exfoliation of AuGrp sheets via the reduction of the Au ions and the growth of the Au NPs (not to scale).

Phytochemicals are polyphenol compounds, obtained from plants, which are composed of benzene and poly hydroxyl groups. In particular, gallic acid (GA) and isoflavone (IF) are polyphenol compounds known to be strong reductants that exhibit antioxidation and anti-inflammatory behavior, and these properties were exploited in the synthesis of biocompatible Au NPs.[16] It should be emphasized that these phytochemicals are used because they are carbon-based materials composed of benzene rings, as is graphene. It is understood that reduction by phytochemicals occurs under milder conditions than those involving other reducing chemicals (e.g., hydrazine or $NaBH_4$); this allows more kinetic and chemical control during the reduction of graphene oxide. Furthermore, many synthetic reductants are highly combustible and/or toxic.[17,18]

In this paper, a novel reduction process for the preparation of AuGrp using phytochemicals (i.e., a mixture of GA and IF) at room temperature with a relatively short processing time (~1 h) is proposed. In our method, Au cations attach to the graphene flakes via the π electrons and are then reduced by phytochemicals without any damage to the graphene structure. The electrical properties of the AuGrp nanocomposites were characterized by electron microscopy, spectroscopy, and a semiconductor-parameter analysis. The exfoliation process occurring during Au-NP growth was simulated using molecular dynamics (MD) software in order to understand the attractive and repulsive forces between the graphene layers and the Au NPs. In addition, photoluminescence enhancement of CdTe quantum dots (QDs) using AuGrp was induced by layer-by-layer (LBL) deposition to make a hybrid device. Furthermore, AuGrp based photoluminescent assay for CFP-10, a tuberculosis antigen (aG), was carried out as a demonstration of a potential application of these materials in a sensing platform.

MATERIAL AND METHODS

AuGrp was synthesized at room temperature using commercially available reagents. $HAuCl_4 \cdot 3H_2O$ and GA were purchased from Sigma-Aldrich Co. (Yongin, Gyeonggi-do). Graphene flakes (model AO-3) were purchased from Graphene Supermarket (Calverton, NY). The average thickness of the graphene flakes was 12 nm, which corresponded to stacks of 30−50 graphene sheets. Furthermore, these flakes were primarily graphitic, so they had an oxygen content of less than 1%. IF was isolated from commercial-grade soybeans. A mixture of GA and IF (the "GI solution") was prepared for use as a reducing agent; 10 mg of IF was dissolved in 10 mL of a 0.01 M GA solution. To make the Au salt solution, we dissolved 0.01 mmol of $HAuCl_4 \cdot 3H_2O$ in 20 mL of deionized (DI) water. Subsequently, 2 mg of graphene-flake powder was added to the Au salt solution. NP intercalation and graphene reduction was carried out in a single flask as follows: First, the mixture of the Au salts and graphene flakes was gently sonicated (Sonics and Materials Inc. VC750, Newtown, CT) using a 5 s on/3 s off routine at a reduced amplification of 20% for 20 min. This treatment produced a black solution because of the dispersion of the flakes. Next, 300 μL of the GI solution was added to the black solution, and this was stirred vigorously for 20 min, during which the color changed to purplish black. This color indicates the production of Au NPs. Exfoliation of the graphene flakes occurred during the reduction step. To further purify this AuGrp solution, we centrifuged the purplish black mixture for 30 min at 8500 rpm to remove byproducts and supernatants.

The absorbance of the AuGrp was measured using UV−vis spectroscopy (SCINCO S310, Daejeon), and the chemical reactions were monitored by FT-IR spectroscopy (JASCO FT-IR 6300, Tokyo). The morphologies and sizes of the nanostructures were characterized

using high-resolution transmission electron microscopy (HR-TEM, JEOL JEM-3010, Tokyo), field-emission scanning electron microscopy (FE-SEM, Hitachi S4700, Tokyo). An X-ray powder diffractometer (XRD, PANalytical Empyrean, Almelo) was used to characterize the AuGrp materials with Cu Kα radiation and a Ni filter. The data were collected over a 2θ range of 20 to 100° at a step size of 0.01° with a collection time of 10 s per step. The electrical conductivity of the AuGrp was analyzed using a semiconductor parameter analyzer (Elecs EL423, Deajeon). Two side-by-side Au electrodes were prepared on a silica wafer, separated by a 20 μm wide channel. An oxygen-plasma treatment was performed for 90 s at 50 W prior to depositing the AuGrp. The current change of the AuGrp-coated area was monitored using linear sweep voltammetry (Elecs EL423, Daegu). The AuGrp and graphene flakes were also analyzed by Raman spectroscopy (Dongwoo Optron, Bundang, Gyeonggi-do). In order to gain further understanding of the formation mechanisms of the AuGrp nanocomposites, a molecular dynamics (MD) simulation was carried out using the Material Studio (MS) v4.2 software (Accelrys, San Diego, CA). Two three-layer structures, which were designed based on our experimental results, were modeled. These two structures were a stacked graphene/small Au particle/graphene structure ("GA1") and a graphene/large Au particle/graphene structure ("GA2").

To demonstrate the possibility of optical applications for these AuGrp materials, we prepared nanoscale thin films of AuGrp and CdTe quantum dots (QDs). To prepare the QDs, we obtained aluminum telluride (Al_2Te_3) from the materion (Mayfield Heights, OH). Cd(ClO_4), cysteamine poly diallyldimethylammonium chloride-(PDDA; M.W. 400 000−500 000) were purchased from Sigma aldrich Co. (Yongin, Gyeonggi-do). The CdTe QDs were synthesized as reported in detail elsewhere[19−22] and coated onto the AuGrp surface. Glass microscope slides (2 × 10 cm^2) were cleaned by immersion in piranha solution (3:1/H_2SO_4:H_2O_2) for 1 h, and then thoroughly rinsed with DI water and stored in DI water prior to use. After oxygen plasma irradiation of the clean glass slide for 90 s, 20 μL of the as-prepared AuGrp solution was dropped onto the glass surface, then the surface was gently washed with ethanol to remove unwanted areas of aggregated AuGrp. To serve as a spacer layer between the AuGrp matrices and the QDs, a 1% PDDA solution was spin coated onto the deposited AuGrp films at 4000 rpm for 40 s and cured at 60 °C for 30 min, forming a nanoscale polymer layer. The spacer layer plays an important role associated with plasmon resonance while also preventing luminescence quenching. 100 μL of the as-prepared QD solution was then deposited onto the PDDA film by spin coating at 40000 rpm for 40 s at room temperature. Aggregation was intentionally suppressed during the coating process by adjusting the quantity of QDs deposited. The photoluminescence (PL) enhancement of the samples was measured using a fluorescence spectrophotometer (Hitachi F-7000, Tokyo, Japan) at an incident angle of 45°. The fluorescence lifetimes (τ) in the samples were measured at a 380 nm excitation wavelength using a light-emitting diode (LED) source (PTI Inc., Edison, NJ).

To evaluate the sensing potential of AuGrp, the photoluminescent immunoassay was demonstrated with CFP-10 tuberculosis (TB) aGs. AuGrp and CdTe QDs of surface were modified with Fab-Antibody (Ab) (i.e., Fab antiCFP-10 and gold binding protein (GBP)-Fab antiCFP-10, depicted as G2 and G3) for selectivity and targeting property. Furthermore, the selectivity test was carried out with Ag85 TB aG. These biomaterials for immunoassay were distributed from Chungnam National University Hospital, Daejeon, Korea. The successful sandwich binding between two different Abs and CFP-10 was cross checked and confirmed by SPR spectroscopy (see Figure S2 in the Supporting Information). The detailed information about biomaterials and procedure for the immunoassay experiments is provided in the Supporting Information.

RESULTS AND DISCUSSION

Figure 1 is a schematic illustration of the AuGrp production process. Because the original graphene flakes possess many π electrons, the gold precursor, i.e., Au^{3+} ions, is able to intercalate into the layered graphene flakes with the assistance of sonication (Step I). To exfoliate the graphene flakes, the Au^{3+} ions were converted into to Au NPs inside the graphene flakes by the addition of the GI solution, a milder reducing agent than $NaBH_4$. $NaBH_4$, a strong reductant, may damage the graphene structure during the exfoliation process via the reduction of graphene oxide because it can reduce the graphene flakes as well as the Au ions.[18] The exfoliation process occurs simultaneously with the conversion of Au ions into Au NPs because of geometric confinement by the graphene layers (Step II). The results of the simulation of these processes are shown in Figure 2.

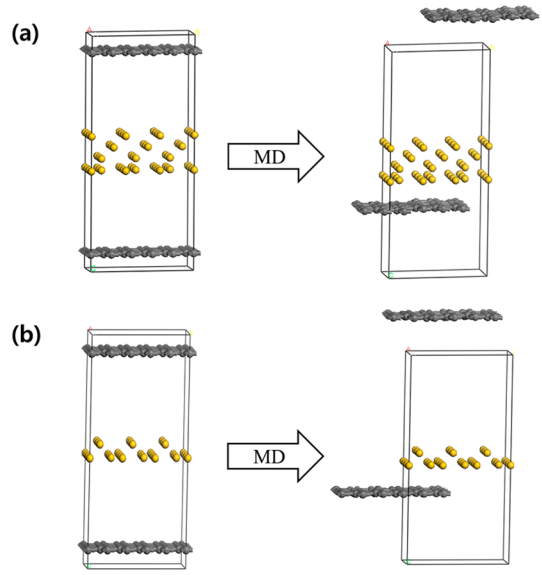

Figure 2. MD simulations of graphene/Au NP interactions. Simulations of graphene exfoliation by (a) large/GA1 and (b) small/GA2 Au NPs. The different panels show the models before and after the simulation.

The two different MD models (GA1 and GA2) were prepared using two graphene layers and Au-NP layers of different heights (the height of the layer corresponds to the NP diameter). The GA1 and GA2 models incorporated large and small NPs, respectively. A three-layer slab structure with periodic boundary conditions was used, based on the schematic illustration of the AuGrp nanocomplex in Figure 1. To investigate the formation mechanisms of the AuGrp, we constructed a representative atomic structure to represent overlapped graphene sheets in the MD simulation. One of the two types of Au layers (large or small) was inserted between two graphene layers with the same spatial extent. A 5000 step energy minimization was then performed to obtain a suitable initial state for simulation. The simulations were conducted under the canonical ensemble (NVT) with a time step of 1 fs for 300 ps until the system reached equilibrium. The MD simulation was continued with a time step of 1 fs for 100 ps for analysis purposes. The results, shown in Figure 2, indicated a significant transformation of the bottom layer of graphene attracted to the Au surface. The upper layer of graphene was repelled from the Au layer toward the end of the MD simulation.

The attraction and repulsion between the Au NPs and graphene layers can be evaluated by calculating their binding

Table 1. Interaction (Attraction/Repulsion) Energies between the Au NPs and Graphene Layers[a].

	GA1			GA2		
MD models	UL[b]-Au NPs	DL[c]-Au NPs	BL[d]	UL[b]-Au NPs	DL[c]-Au NPs	BL[d]
E_{total}	1.359×10^5	1.357×10^5	5.291×10^3	6.711×10^5	6.670×10^5	5.329×10^3
$E_{graphene}$	2.612×10^3	2.604×10^3	2.613×10^3	2.623×10^3	2.621×10^3	2.623×10^3
$E_{Au\ or\ graphene}$	1.333×10^5	1.333×10^5	2.603×10^3	6.676×10^5	6.676×10^5	2.621×10^3
$E_{binding}$	3.077×10^1	1.911×10^2	-7.52×10^2	3.812×10^1	2.255×10^2	-8.548×10^1

[a]Units: kcal mol^{-1}. [b]UL: up-layer of graphene. [c]DL: down-layer of graphene. [d]Both graphene layers without Au NPs (the slight difference in energy results from instability of the initial state).

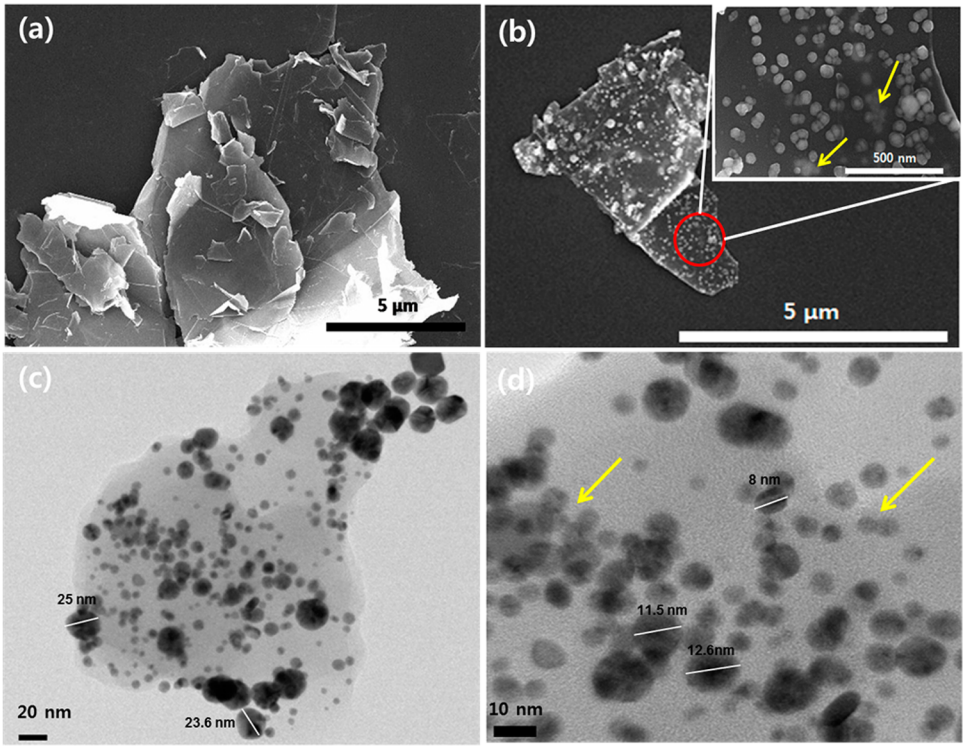

Figure 3. Electron microscopy analysis of the graphene and AuGrp materials. SEM images of (a) as-received graphene flakes and (b) AuGrp nanocomposites. (c, d) TEM images of the AuGrp materials. The yellow arrows in b and d indicate NPs on the underside of the graphene sheets.

energy. Table 1 gives the binding energies between the Au NPs and each graphene layer, which were calculated using

$$E_{binding} = (E_{graphene} + E_{AuNPs}) - E_{total} \quad (1)$$

where $E_{graphene}$ is the energy of the graphene layer, E_{AuNPs} is the energy of the Au NPs, and E_{total} is the energy of the graphene layer with Au NPs. Note that a high binding energy indicates a high adhesive or repulsive strength between the Au NPs and the graphene layer, and the ± signals in front of the numbers indicate the nature of the force, i.e., whether it is attractive (+) or repulsive (−).[23] The binding energies were calculated using the condensed-phase optimized molecular potentials for atomistic simulation studies (COMPASS) force field, and the results are listed in Table 1. From the results of the computational simulation, the graphene/graphene binding energy without an inserted Au NP layer (denoted "BL") was slightly negative; this may be a computational artifact due to the fact that the model maintained a fixed distance between the two layers, which requires a repulsive force. The results from both BL simulations were identical. When an Au layer was inserted between the two graphene layers, the binding energies between each layer of graphene and the Au NPs were found to be positive values, i.e., attractive forces predominated. The binding forces of the two graphene sheets with the Au NP layer were significantly different. This is because one graphene layer was attracted to Au NP layers, which resulted in the decoration of the graphene layer with Au NPs (i.e., AuGrp). The other layer was repelled, and was simultaneously exfoliated. It should be noted that the top and bottom layer of graphene are computationally identical, and the binding energy increased slightly with NP size. The computational and experimental results are consistent, reinforce each other, and demonstrate the success of our novel synthesis mechanism for the simultaneous decoration and exfoliation of graphene.

Figure 3 presents electron microscope images of the as-received graphene flakes and the graphene after the two-step treatment outlined in Figure 1, i.e., the AuGrp. The commercial graphene flakes had many layers and a maximum size of 5 μm, as shown in Figure 3a. The flake thickness was 12 nm, on average, which corresponded to 30 to 50 monolayers. Figure 3b shows the exfoliated graphene decorated with Au NPs. The surfaces of the graphene sheets were covered homogeneously with a large number of Au NPs over a large area (~5 μm); this is because of the large number of surface charges associated with the GI hydroxyl groups that function as a stabilizer. The

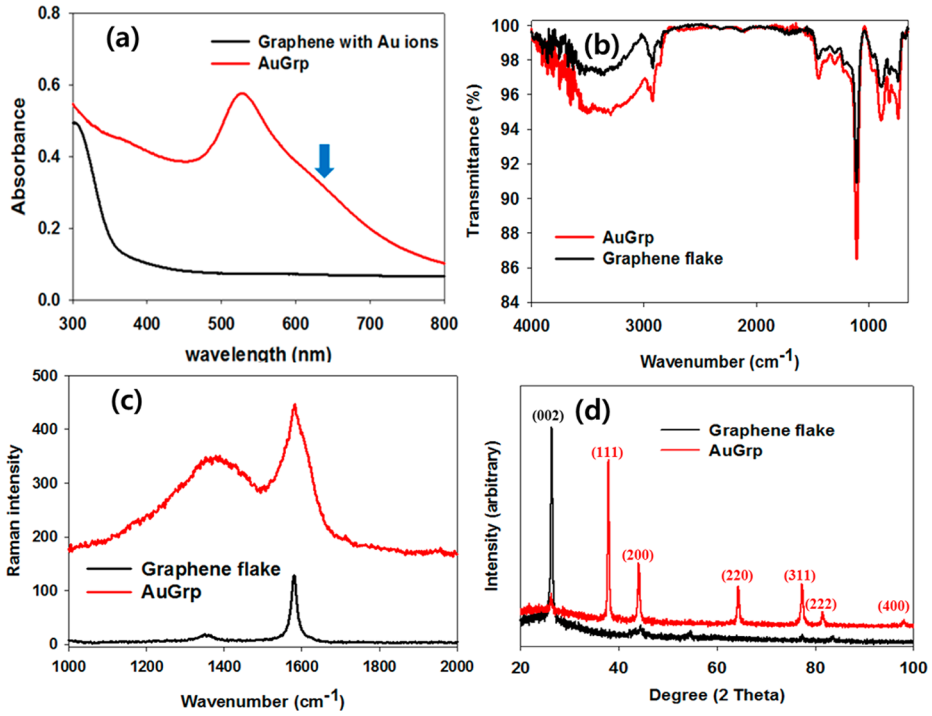

Figure 4. Chemical and structural analysis of the graphene and AuGrp materials. (a) UV−vis absorption spectra of graphene flakes impregnated with Au ions and of AuGrp. (b) FT-IR spectra, (c) Raman spectra, and (d) XRD patterns of as-received graphene flakes and AuGrp.

strong repulsive force that these charges provided prevented the agglomeration of Au NPs. The graphene layer is flexible, and folds in the sheet can be observed in the SEM images. The sheet structure was not damaged during the exfoliation process. Au NPs on the opposite-facing side of AuGrp sheet were observed at low SEM accelerating voltage (15 keV); however, these were out of focus (Figure 3b, inset, yellow arrows).

A TEM study was performed on the same sample. Great care was required because the high voltage electron source can damage the graphene structure. Because the carbon structure of graphene is transparent and heavy metals have high electron absorption, Au NPs were easily distinguished in the TEM images in Figures 3c, d. Indeed, many Au NPs were observed on the surface of graphene sheets in this way. The thickness of the layers within the graphene sheet was determined by weak changes in contrast in the TEM images. The large NPs were mostly located along the edges of the AuGrp sheets; this may be the result of an inhomogeneous distribution of intercalating Au ions and reductant between the graphene sheets, when considered at the nanoscale. Furthermore, the reactivity may vary depending on the location on the graphene sheets, i.e., on the edges or in the middle of a sheet, due to variations in the interaction forces between the Au NPs and graphene layers. Thus, the sizes of AuNPs on the graphene were not highly uniformed from a few nanometers on middle part to maximum 25 nm on edge side of graphene (Figure 3c, d). However, Au NPs were well dispersed on the graphene sheet evenly without surfactant treatment such as CTAB. In the highly magnified TEM image of Figure 3d, the location of Au NPs on the underside of the sheet can be also distinguished, as was the case with the SEM images. An energy-dispersive X-ray spectroscopy (EDS) analysis was performed during imaging, and these results are provided in Figure S1 (see the Supporting Information). The Au peaks in the EDS spectrum were correlated in space with the positions of the Au NPs on the graphene surface, and the C peak was produced by graphene. The other peaks, such as Mg, Na, and Ca, were associated with the glass slide.

The optical absorbance of the AuGrp was characterized using UV−vis spectroscopy. Figure 4a shows a strong absorbance peak at 525 nm in the UV−vis spectrum, which is typical of the plasmonic band of Au NPs. A second plasmonic band was also observed at 625 nm (indicated by the blue arrow). Generally, the presence of a second band is associated with plasmonic interactions among noble-metal NPs, e.g., the longitudinal direction of one-dimensional nanostructures.[24] In our experiments, it is reasonable to conclude that this band is correlated with plasmonic resonance localized near the Au NPs, as well as interaction between the graphene base and the electron clouds of the Au NPs they are decorated with.[25] The SPR of individual Au NPs may be influenced by adjacent Au NPs. The interaction of the electron clouds may be due to the orbital overlap of π electrons on the graphene surface, which resulted in a slight shoulder at 625 nm. However, in the case of graphene with intercalated Au ions, no plasmon band was observed.

A functional-group analysis was carried out using FT-IR spectroscopy, and the resulting spectrum is shown in Figure 4b. The bands located in the range 1450−1580 cm^{-1} are characteristic of the aromatic bonds of graphene. The C−O single-bond vibration was observed at 1080 cm^{-1}. The alkane and alkene chains present in graphene typically result in the appearance bands in the range 2800−3000 cm^{-1} and 3000−3100 cm^{-1}, respectively. The hydroxyl group band can be observed at 3300 cm^{-1}. The spectrum of the AuGrp was similar to that of the as-received graphene flakes because the Au NPs are covered with phytochemicals. Thus, methoxy (C−O and O−H) groups were clearly observable as distinct peaks in the spectra. It should be emphasized that there were no specific bands or peak intensity enhancements related to damage in the

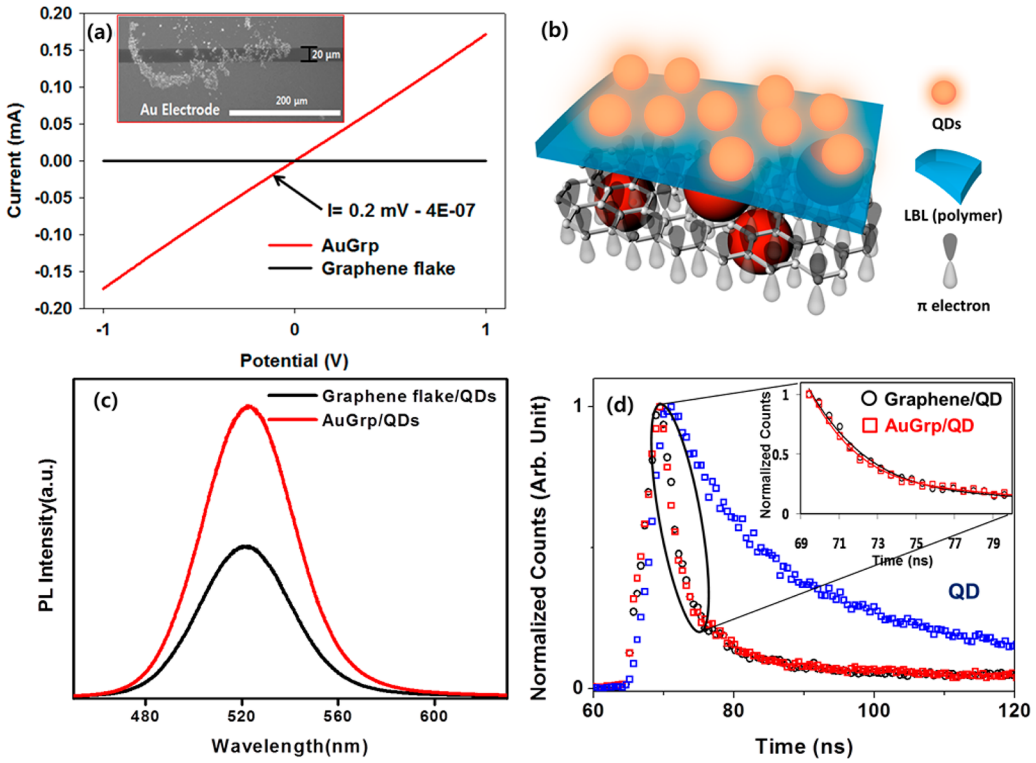

Figure 5. Electrical and plasmonic properties of the graphene and AuGrp materials. (a) Current−potential curves of the AuGrp and graphene flake devices with 20 μm gap. Inset: SEM image of the device structure. (b) Graphical representation of the AuGrp/QD hybrid films. (c) PL spectra, and (d) lifetime (τ) profiles of graphene flakes and AuGrp after CdTe-NP deposition.

structure of graphene such as the bands around 1680 cm^{-1} that indicate the presents of allyl groups.[18]

Figure 4c shows the Raman spectra of graphene and AuGrp at an excitation wavelength of 514 nm. In both spectra, the D peak can be observed at 1340 cm^{-1}, and a G peak is visible around 1580 cm^{-1}. The intensity of the spectrum of AuGrp is four times greater than that of the graphene flakes. This surface-enhanced Raman scattering effect was induced by the Au NPs that decorated the graphene surface.[13]

Powder XRD was used to characterize the structure of the AuGrp, and the results are shown in Figure 4d. In the graphene flake samples (black line), the strong diffraction peak at 2θ = 26.2° was identified as the (002) plane of graphite (ICSD card no: 01−075−1621). After decorating the graphite with Au NPs, several new diffraction peaks were observed (red line), and the carbon peak persisted at 2θ = 26.2°. The presence of crystalline Au in the AuGrp was confirmed by the presence of the characteristic diffraction peaks of the face-centered cubic structure of bulk Au, i.e., (111), (200), (220), (311), (222), and (400) planes at 2θ values of 38.2, 44.4, 64.6, 77.5, 81.7, and 98.1°, respectively (ICSD card no: 00−004−0784).

The electrical resistance of the AuGrp and graphene flakes was measured using two Au electrodes on a silicon wafer with a 20-μm gap, as shown in Figure 5a (a SEM image of the device is shown inset). The average resistance of AuGrp was ∼5 kΩ, and that of the graphene flakes was much higher. Many other researchers have reported the electrical resistance of graphene materials; the resistances of graphene oxide (GO) and reduced GO are typically in the MΩ range, and that of multilayer Langmuir−Blodgett film is 8−150 kΩ.[26,27] Even some decorated graphene materials, such as those incorporating TiO_2 or Cu NPs, have electrical resistances >30 kΩ.[28] Even though data from experiments conducted under different conditions may not be directly comparable, our electrical resistance was 5−30 times lower than that reported for any decorated graphene material and 1000 times lower than that reported for GO or reduced GO. It is probable that the low resistance of the AuGrp results from the interaction between the unlocalized π electrons of graphene and the highly conductive electron clouds of Au NPs, as illustrated in Figure 5b.[9]

To demonstrate the effect of AuGrp on the PL intensities of QDs, which was studied to shed light on potential plasmonic applications of AuGrp, we prepared AuGrp/QD films using a LBL method. Figure 5b illustrates the geometry of the hybrid device. The fluorescent QDs were deposited on the polymer layer that was spin-coated onto the AuGrp. Figure 5c shows the PL spectra obtained from the QDs on the two different surfaces, i.e., the as-received graphene flakes and the AuGrp, at an excitation wavelength of 380 nm. An approximately 2-fold PL enhancement from the QDs on the surface of AuGrp was observed compared to the PL intensity on the as-received graphene surface. PL decay was measured using a 380 nm excitation LED source at room temperature. Figure 5d shows the PL-lifetime profiles of the QDs on the two different surfaces. After excitation, the PL lifetime decreased sharply in both substrates. The PL-lifetime decay of the QDs on the AuGrp surface was especially faster than that on the as-received graphene surface. The decay rate on the AuGrp surface (red square) was 1.807 ± 0.094 ns, and that on the graphene flake surface (blue circle) was 2.082 ± 0.104 ns. Generally, when plasmon resonance energy transfer occurs between plasmonic materials and fluorescent materials, a simultaneous decrease in exciton lifetime and enhanced PL intensity are observed in

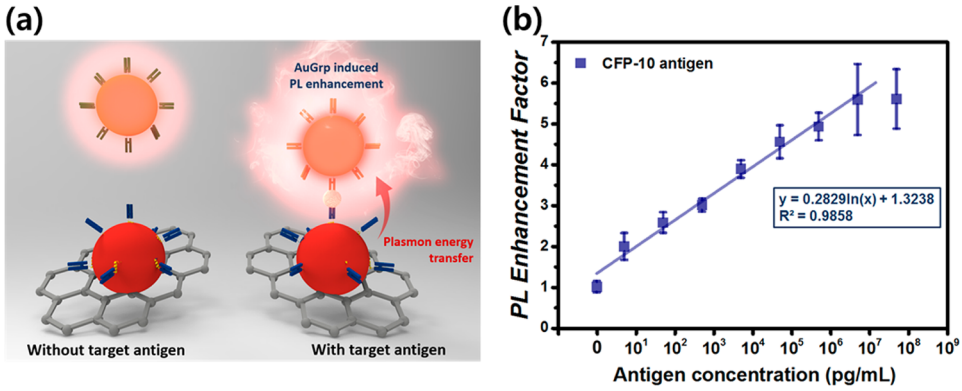

Figure 6. AuGrp-based immunoassay platform performance. (a) Schematic illustration of the immunoassay mechanism with AuGrp as the sensing platform. (b) Sensitivity of the QD-decorated AuGrp immunoassay device. The PL enhancement factor is defined as the ratio of the enhanced PL intensity to the PL intensity of a negative control (i.e., lacking aG).

fluorescent materials; this is the case in Figures 5c, d. Moreover, the shorter decay of lifetime in QDs could be caused by electrons which drop quickly from the excitation state to valence state, and the majority of energy is converted not into heat but into fluorescence. In our system, it is probable that the PL enhancement of QDs was due to the plasmonic effect of the Au NPs. However, the enhancement ratio and lifetime did not vary significantly compared with similar experiments on plasmonic interactions with Au NPs.[29] This is because of the electron interaction between Au NPs and graphene, in which the electron clouds of NPs were degenerated with graphene π electrons, as observed in the UV−vis spectra (cf. Figure 4a). The degenerated electron cloud weakens plasmon localization, which results in weak plasmon-induced enhancement.

Finally, we demonstrated target aG detection by means of sandwich-type immunoassay based on the AuGrp-induced PL enhancement present in the AuGrp/CdTe QDs.[30] In the presence of the TB aG (CFP-10), the CdTe probes would be captured by the AuGrp sandwich platform due to the aG-Ab interaction and plasmonic energy transfer from the AuGrp to the CdTe probes, would produce PL enhancement, as shown in Figure 6a. In addition, the enhancement of PL intensity, expressed by the PL enhancement factor, (PLEF, E_{PL}) defined as $E_{PL} = PL_{target\ aG}/PL_{without\ aG}$, increased with the concentration of target aG (CFP-10) over the range 5.1 pg/mL to 51 μg/mL, as shown in Figure 6b. Using a linear regression based on the AuGrp-induced PL enhancement over the linear range of the data in Figure 6b, a relationship between the CFP-10 concentration and the PLEF was determined as

$$E_{PL} = 0.2829\ln[\mathrm{CFP} - 10] + 1.3238\ (R^2 = 0.9858) \quad (2)$$

On the basis of this sensing platform, the calculated detection limit was 4.5 pg/mL for CFP-10 (see eqs S1 and S2 in the Supporting Information), on the other hands, enhancement of PL was not measured without CFP-10 (see Figure S3 in the Supporting Information). Furthermore, the selectivity test of AuGrp-based immunosensing was demonstrated with the other TB aG, Ag85. The PLEF was also monitored with a similar range of Ag85 concentrations; however, this aG was not influence by the detection system (see Figure S4 in the Supporting Information). The CFP-10 Ab modified AuGrp could be targeted to only CFP-10, and thus Ag85 should not be detected. Recently TB symptom has been monitored by mycobacteria growth indicator tube (MGIT) or polymerase chain reaction (PCR) test. These processes are highly sensitive, but time - consuming technique since it requires over 10 days for TB diagnosis.[31] To make it worse, these techniques are not suitable to distinguish *Mycobacterium tuberculosis* (MTB) and nontuberculous mycobacteria (NTM).[32] Thus, to overcome these disadvantages, researchers have developed many different TB sensing systems to show rapid detection, and high sensitivity and selectivity using direct clues, e.g., secreted antigens of TB virus such as CFP-10 biomarker. Many trials to monitor antigens have been performed where different detection limitations were observed; for example, surface plasmonic resonance (SPR) spectroscopy (~100 ng/mL),[33] matrix-assisted laser desorption/ionization time-of-flight mass spectrometry (MALDI-TOF MS) analysis with nanodiamonds (~90 ng/mL),[34] enzyme-linked immunosorbent assay (ELISA) (~60 pg/mL),[35] and magnetophoresis process with iron oxide and Au NPs (~10 pg/mL).[31] Comparing with recent progress of the monitoring system, our AuGrp based sandwich-type immunoassay exhibited higher sensitivity and selectivity in target aG detection.

CONCLUSIONS

AuGrp was fabricated using a phytochemical-assisted synthesis lacking harsh thermal conditions or reducing agents. According to an electron microscopy analysis, Au NPs were dispersed evenly on both sides of the graphene sheets. A two-step mechanism was suggested, in which the intercalation of Au ions is followed by exfoliation of the graphene sheets as the Au ions are converted to Au NPs. The UV−vis spectrum indicated a localized SPR effect at the AuGrp surface. The electrical conductivity of graphene is greatly enhanced by Au NP decoration, as compared with all other graphene structures reported so far. The NP synthesis and induced exfoliation process was computationally simulated to provide a deeper understanding of the underlying mechanism. These results revealed that there were attractive and repulsive forces between the two graphene layers that enable the simultaneous decoration with Au NPs and exfoliation of the graphene sheets. In order to demonstrate sensing application, TB aG was monitored by plasmon induced photoluminescent assay with various concentration of CFP-10 and the detection limit is 4.5 pg/mL. In addition, this technic showed high selectivity against Ag85. Therefore, AuGr- based sensing platform exhibited the potential for biosensor application with high sensitivity and selectivity.

■ ASSOCIATED CONTENT

Supporting Information

The supplementary methods for AuGrp modification with TB Ab (anti CFP-10), and detection process of TB aGs, EDS spectrum of AuGrp, SPR spectra for conformation of CFP-10 sandwich structure, feasibility of the detection of aGs (CFP-10) with AuGrp, and selectivity results of AuGrp with Ag85 aGs. This material is available free of charge via the Internet at http://pubs.acs.org/

■ AUTHOR INFORMATION

Corresponding Author

*E-mail: jaebeom@pusan.ac.kr. Tel: (+82) 55-350-5298. Fax: (+82) 55-350-5299.

Notes

The authors declare no competing financial interest.

■ ACKNOWLEDGMENTS

This research was supported by the Korea Healthcare Technology R&D Project, Ministry of Health & Welfare, Republic of Korea (HI13C0862); from the Civil & Military Technology Cooperation Program through the National Research Foundation of Korea (NRF) (No. 2013M3C1A9055407); and from Korea-Japan International Collaboration Program through the NRF funded by the Ministry of Science, ICT & Future Planning (No. 2014K2A2A4001081).

■ REFERENCES

(1) Tassin, P.; Koschny, T.; Kafesaki, M.; Soukoulis, C. M. A Comparison of Graphene, Superconductors and Metals as Conductors for Metamaterials and Plasmonics. *Nat. Photonics* **2012**, *6*, 259−264.

(2) Kumar, R.; Singh, R. K.; Singh, J.; Tiwari, R. S.; Srivastava, O. N. Synthesis, Characterization and Optical Properties of Graphene Sheets-ZnO Multipod Nanocomposites. *J. Alloy. Compd.* **2012**, *526*, 129−134.

(3) Zhang, M.; Yuan, R.; Chai, Y.; Chen, S.; Zhong, H.; Wang, C.; Cheng, Y. A Biosensor for Cholesterol Based on Gold Nanoparticles-Catalyzed Luminol Electrogenerated Chemiluminescence. *Biosens. Bioelectron.* **2011**, *32*, 288−292.

(4) Wang, Y.; Zhang, S.; Du, D.; Shao, Y. Y.; Li, Z. H.; Wang, J.; Engelhard, M. H.; Li, J. H.; Lin, Y. H. Self Assembly of Acetylcholinesterase on a Gold Nanoparticles-Graphene Nanosheet Hybrid for Organophosphate Pesticide Detection Using Polyelectrolyte as a Linker. *J. Mater. Chem.* **2011**, *21*, 5319−5325.

(5) Choi, B. G.; Hong, J.; Hong, W. H.; Hammond, P. T.; Park, H. S. Facilitated Ion Transport in All-Solid-State Flexible Supercapacitors. *ACS Nano* **2011**, *5*, 7205−7213.

(6) Hong, H.; Yang, K.; Zhang, Y.; Engle, J. W.; Feng, L. Z.; Yang, Y. A.; Nayak, T. R.; Goel, S.; Bean, J.; Theuer, C. P.; Barnhart, T. E.; Liu, Z.; Cai, W. B. In Vivo Targeting and Imaging of Tumor Vasculature With Radiolabeled, Antibody-Conjugated Nanographene. *ACS Nano* **2012**, *6*, 2361−2370.

(7) Gong, J. M.; Zhou, T.; Song, D. D.; Zhang, L. Z. Monodispersed Au Nanoparticles Decorated Graphene as an Enhanced Sensing Platform for Ultrasensitive Stripping Voltammetric Detection of Mercury(II). *Sens. Actuator B-Chem.* **2010**, *150*, 491−497.

(8) Liu, J. B.; Li, Y. L.; Li, Y. M.; Li, J. H.; Deng, Z. X. Noncovalent DNA Decorations of Graphene Oxide and Reduced Graphene Oxide toward Water-Soluble Metal-Carbon Hybrid Nanostructures via Self-Assembly. *J. Mater. Chem.* **2010**, *20*, 900−906.

(9) Bei, F. L.; Hou, X. L.; Chang, S. L. Y.; Simon, G. P.; Li, D. Interfacing Colloidal Graphene Oxide Sheets with Gold Nanoparticles. *Chem.—Eur. J.* **2011**, *17*, 5958−5964.

(10) Xiang, J. L.; Drzal, L. T. Electron and Phonon Transport in Au Nanoparticle Decorated Graphene Nanoplatelet Nanostructured Paper. *ACS Appl. Mater. Interfaces* **2011**, *3*, 1325−1332.

(11) Yang, X.; Xu, M.; Qiu, W.; Chen, X.; Deng, M.; Zhang, J.; Iwai, H.; Watanabe, E.; Chen, H. Graphene Uniformly Decorated with Gold Nanodots: In Situ Synthesis, Enhanced Dispersibility and Applications. *J. Mater. Chem.* **2011**, *21*, 8096−8103.

(12) Jasuja, K.; Linn, J.; Melton, S.; Berry, V. Microwave-Reduced Uncapped Metal Nanoparticles on Graphene: Tuning Catalytic, Electrical, and Raman Properties. *J. Phys. Chem. Lett.* **2010**, *1*, 1853−1860.

(13) Fu, X.; Bei, F.; Wang, X.; O'Brien, S.; Lombardi, J. R. Excitation Profile of Surface-Enhanced Raman Scattering in Graphene-Metal Nanoparticle Based Derivatives. *Nanoscale* **2010**, *2*, 1461−1466.

(14) Goncalves, G.; Marques, P. A. A. P.; Granadeiro, C. M.; Nogueira, H. I. S.; Singh, M. K.; Gracio, J. Surface Modification of Graphene Nanosheets with Gold Nanoparticles: The Role of Oxygen Moieties at Graphene Surface on Gold Nucleation and Growth. *Chem. Mater.* **2009**, *21*, 4796−4802.

(15) Hong, W. J.; Bai, H.; Xu, Y. X.; Yao, Z. Y.; Gu, Z. Z.; Shi, G. Q. Preparation of Gold Nanoparticle/Graphene Composites with Controlled Weight Contents and Their Application in Biosensors. *J. Phys. Chem. C* **2010**, *114*, 1822−1826.

(16) Lee, J.; Kim, H. Y.; Zhou, H.; Hwang, S.; Koh, K.; Han, D. W.; Lee, J. Green Synthesis of Phytochemical-Stabilized Au Nanoparticles Under Ambient Conditions and Their Biocompatibility and Antioxidative Activity. *J. Mater. Chem.* **2011**, *21*, 13316−13326.

(17) Schmidt, E. W. *Hydrazine and Its Derivatives: Preparation, Properties, Applications*, 2nd ed.; Wiley−Interscience: New York, 2001.

(18) Fernandez-Merino, M. J.; Guardia, L.; Paredes, J. I.; Villar-Rodil, S.; Solis-Fernandez, P.; Martinez-Alonso, A.; Tascon, J. M. D. Vitamin C Is an Ideal Substitute for Hydrazine in The Reduction of Graphene Oxide Suspensions. *J. Phys. Chem. C* **2010**, *114*, 6426−6432.

(19) Gaponik, N.; Talapin, D. V.; Rogach, A. L.; Hoppe, K.; Shevchenko, E. V.; Kornowski, A.; Eychmuller, A.; Weller, H. Thiol-Capping of CdTe Nanocrystals: An Alternative to Organometallic Synthetic Routes. *J. Phys. Chem. B* **2002**, *106*, 7177−7185.

(20) Lee, J.; Orazbayev, A.; Govorov, A. O.; Kotov, N. A. Solvent Effect in Dynamic Superstructures from Au Nanoparticles and CdTe Nanowires: Experimental Observation and Theoretical Description. *J. Phys. Chem. C* **2010**, *114*, 1404−1410.

(21) Lee, J.; Chen, H.; Koh, K.; Chang, C. L.; Kim, C. M.; Kim, S. H. Nanoassembly of CdTe Nanowires and Au Nanoparticles: pH Dependence and Reversibility of Photoluminescence. *Korean J. Chem. Eng.* **2009**, *26*, 417−421.

(22) Lee, J.; Govorov, A. O.; Kotov, N. A. Nanoparticle Assemblies with Molecular Springs: A Nanoscale Thermometer. *Angew. Chem., Int. Ed.* **2005**, *117*, 7605−7608.

(23) Zhou, H.; Gao, Y.; Hwang, S.; Lee, D.; Park, J. Y.; Lee, J. A Novel Approach to Controlling CaCO3 Crystalline Assembly by Changing the Concentration of Poly (aspartic acid). *Bull. Korean Chem. Soc.* **2011**, *32*, 4027−4034.

(24) Lee, J.; Zhou, H.; Lee, J. Small Molecule Induced Self-Assembly of Au Nanoparticles. *J. Mater. Chem.* **2011**, *21*, 16935−16942.

(25) Lee, Y. H.; Polavarapu, L.; Gao, N.; Yuan, P.; Xu, Q. H. Enhanced Optical Properties of Graphene Oxide-Au Nanocrystal Composites. *Langmuir* **2012**, *28*, 321−326.

(26) Shin, H. J.; Kim, K. K.; Benayad, A.; Yoon, S. M.; Park, H. K.; Jung, I. S.; Jin, M. H.; Jeong, H. K.; Kim, J. M.; Choi, J. Y.; Lee, Y. H. Efficient Reduction of Graphite Oxide by Sodium Borohydrilde and Its Effect on Electrical Conductance. *Adv. Funct. Mater.* **2009**, *19*, 1987−1992.

(27) Park, S.; Ruoff, R. S. Chemical Methods for the Production of Graphenes. *Nat. Nanotechnol.* **2009**, *4*, 217−224.

(28) Luechinger, N. A.; Athanassiou, E. K.; Stark, W. J. Graphene-Stabilized Copper Nanoparticles as an Air-Stable Substitute for Silver and Gold in Low-Cost Ink-Jet Printable Electronics. *Nanotechnology* **2008**, *19*, 445201.

(29) Lee, J.; Hernandez, P.; Lee, J.; Govorov, A. O.; Kotov, N. A. Exciton-Plasmon Interactions in Molecular Spring Assemblies of Nanowires and Wavelength-Based Protein Detection. *Nat. Mater.* **2007**, *6*, 291−295.
(30) Lee, J.; Ahmed, S. R.; Oh, S.; Kim, J.; Suzuki, T.; Parmar, K.; Park, S. S.; Lee, J.; Park, E. Y. A Plasmon-Assisted Fluoro-Immunoassay Using Gold Nanoparticle-Decorated Carbon Nanotubes for Monitoring the Influenza Virus. *Biosens. Bioelectron.* **2015**, *64*, 311−317.
(31) Kim, J.; Lee, J.; Lee, K. I.; Park, T. J.; Kim, H. J.; Lee, J. Rapid Monitoring of CFP-10 During Culture of Mycobacterium Tuberculosis By Using a Magnetophoretic Immunoassay. *Sens. Actuator, B* **2013**, *177*, 327−333.
(32) Nyendak, M. R.; Lewinsohn, D. A.; Lewinsohn, D. M. New Diagnostic Methods for Tuberculosis. *Curr. Opin. Infect. Dis.* **2009**, *22*, 174−182.
(33) Hong, S. C.; Chen, H. X.; Lee, J.; Park, H. K.; Kim, Y. S.; Shin, H. C.; Kim, C. M.; Park, T. J.; Lee, S. J.; Koh, K.; Kim, H. J.; Chang, C. L.; Lee, J. Ultrasensitive Immunosensing of Tuberculosis CFP-10 Based on SPR Spectroscopy. *Sens. Actuator B-Chem.* **2011**, *156*, 271−275.
(34) Soo, P. C.; Kung, C. J.; Horng, Y. T.; Chang, K. C.; Lee, J. J.; Peng, W. P. Detonation Nanodiamonds for Rapid Detection of Clinical Isolates of Mycobacterium Tuberculosis Complex in Broth Culture Media. *Anal. Chem.* **2012**, *84*, 7972−7978.
(35) Feng, T. T.; Shou, C. M.; Shen, L.; Qian, Y.; Wu, Z. G.; Fan, J.; Zhang, Y. Z.; Tang, Y. W.; Wu, N. P.; Lu, H. Z.; Yao, H. P. Novel Monoclonal Antibodies to ESAT-6 and CFP-10 Antigens for ELISA-Based Diagnosis of Pleural Tuberculosis. *Int. J. Tuberc. Lung Dis.* **2011**, *15*, 804−810.